Climate Dynamics (2004) 22: 539–553
DOI 10.1007/s00382-004-0396-y

S. L. Weber · T. J. Crowley · G. van der Schrier

Solar irradiance forcing of centennial climate variability during the Holocene

Received: 27 June 2003 / Accepted: 8 January 2004 / Published online: 24 March 2004

Abstract Centennial climate variability during the Holocene has been simulated in two 10,000 year experiments using the intermediate-complexity ECBilt model. ECBilt contains a dynamic atmosphere, a global 3-D ocean model and a thermodynamic sea-ice model. One experiment uses orbital forcing and solar irradiance forcing, which is based on the Stuiver et al. residual ^{14}C record spliced into the Lean et al. reconstruction. The other experiment uses orbital forcing alone. A glacier model is coupled off-line to the climate model. A time scale analysis shows that the response in atmospheric parameters to the irradiance forcing can be characterised as the direct response of a system with a large thermal inertia. This is evident in parameters like surface air temperature, monsoon precipitation and glacier length, which show a stronger response for longer time scales. The oceanic response, on the other hand, is strongly modified by internal feedback processes. The solar irradiance forcing excites a (damped) mode of the thermohaline circulation (THC) in the North Atlantic Ocean, similar to the loop-oscillator modes associated with random-noise freshwater forcing. This results in a significant peak (at time scales 200–250 year) in the THC spectrum which is absent in the reference run. The THC response diminishes the sea surface temperature response at high latitudes, while it gives rise to a signal in the sea surface salinity. A comparison of the model results with observations shows a number of encouraging similarities.

S. L. Weber (✉) · G. van der Schrier
Royal Netherlands Meteorological Institute (KNMI),
PO Box 201, 3730 AE De Bilt, The Netherlands
E-mail: weber@knmi.nl

T. J. Crowley
Duke University, Durham, North Carolina, USA

1 Introduction

Numerous studies have found evidence of solar irradiance forcing in proxy records of different climatic parameters, covering different time intervals during the Holocene and representative of different seasons and spatial scales. Simulations with coupled general circulation models (GCMs) indicate that solar forcing indeed dominates over internal variability in generating temperature variations at decadal and longer time scales and large spatial scales (Cubasch et al. 1997; Drijfhout et al. 1999; Rind et al. 1999). All of these studies are restricted to annual-decadal variability of the last 500–1000 years.

Consideration of longer time scales (50 years and longer) is of great interest. First, many proxy data have low temporal resolution, so that they registrate only the longer time scales (e.g., Bond et al. 2001). Second, the solar forcing spectrum is thought to be red with a number of spectral peaks (Stuiver and Braziunas 1993; Lean et al. 1995). Third, the climatic response to a radiative forcing is attenuated due to the thermal inertia of the oceans when the period of the forcing is small compared to the response time scale of the oceans (White et al. 1998). This assumes a direct response, where internal feedback processes do not play an important role. The low-frequency components in the forcing are thus expected to be more efficient than the high-frequency components. In addition, they have higher amplitudes.

Estimated solar irradiance changes throughout the Holocene have been used to force an atmosphere–ocean model of intermediate-complexity (ECBilt). The solar forcing is based on residual ^{14}C values from tree rings (Stuiver et al. 1998) over the last 10,000 years. It has decadal resolution. This record is spliced into the Lean et al. (1995) estimate of historic irradiance variations in order to obtain a scaling factor (compare Crowley 2000). The aim of the present study is to assess the role of solar forcing in generating Holocene climate variability. This

extends earlier modeling studies to longer time scales. In addition, we more thoroughly analyze the ocean response than previous authors and we consider glacier length as an example of a combined temperature and precipitation signal. We include orbital forcing (Berger 1978) and compare the present simulation to a 10,000 year reference experiment with orbital forcing alone (Weber 2001). Both experiments use the present-day control climate as the initial state. Other forcings (like volcanic dust or changes in greenhouse gas concentrations) are neglected.

The present study is restricted to the possible climatic impacts of total irradiance variations, independent of wavelength. Recent work has shown that variations in UV irradiance can modify atmospheric modes of variability through changes in the radiative and dynamical coupling of the stratosphere and troposphere (e.g., Shindell et al. 2001; Toupali et al. 2003). However, this approach is at present not feasible in long-term climate variability studies. First, the spectrum of irradiance variability is not known for longer time scales. Second, stratosphere/troposphere models are too time-consuming to allow for long-term experiments even though they are coupled to a mixed-layer ocean. The present study is to a certain extent complementary to this approach, as it includes a dynamic ocean (versus a mixed layer) and has its focus on large-scale (versus regional) climatic impacts.

The climate model ECBilt and the experimental design used are discussed in Sect. 2, where we also compare the climatic sensitivity and signal-to-noise ratio simulated by ECBilt with that of more comprehensive GCMs and data. In the following sections we consider the climatic response as a function of time scale, computing correlations with the solar forcing for a range of band-pass filter periods. The response in atmospheric parameters is analyzed in Sect. 3.1, while glacier length as computed with an off-line glacier model is analyzed in Sect. 3.2. The oceanic response is analyzed in Sect. 4. Section 5 gives a summary and discussion.

2 Climate model and experimental design

2.1 The ECBilt coupled model

The atmospheric component of the global climate model ECBilt (Opsteegh et al. 1998) is a moist dynamic model based on the quasi-geostrophic equations. An estimate of the neglected ageostrophic terms is included, which results in a reasonable simulation of the tropical circulation cells and monsoon precipitation. However, the amplitude of the tropical circulation is too weak and variability is considerably underestimated. There are no ENSO events. The model incorporates orography, simplified representations of the diabatic-heating processes and the hydrological cycle. There is a land surface parametrization, based on a bucket model for soil moisture and a thermodynamic snow model. There is no representation of cloud dynamics, but cloud cover is prescribed from seasonal climatology.

The atmospheric component is synchronously coupled to a dynamic ocean model and a thermodynamic sea-ice model. The resolution in the atmosphere is (T21, L3), while the flat-bottom ocean component has comparable horizontal resolution (5.6° × 5.6°) and 12 unevenly spaced vertical levels. The land-sea mask has realistic geometry. No flux corrections are used, apart from a correction in the freshwater flux in the Arctic Ocean to compensate excessive precipitation in this region. In terms of complexity, the coupled model lies in the upper range of Earth system models of intermediate complexity (Claussen et al. 2002). It is computationally efficient, with a 10,000-year simulation taking about 10 weeks computing time on a workstation.

Solar forced runs have previously been conducted with ECBilt using idealized irradiance variations (Drijfhout et al. 1999) and using estimates of historic solar forcing for the last millenium (Van der Schrier et al. 2002). Studies on the impact of orbital forcing with ECBilt include Weber (2001), Weber and Oerlemans (2003) and Tuenter et al. (2003), while a later model version with interactive vegetation was used by Renssen et al. (2001, 2003). The ECBilt response at the mid-Holocene optimum was compared with other coupled model results by Braconnot et al. (2003).

2.2 Solar forcing of the climate of the last millenium

In addition to the 10,000 year experiments described in the following sections, we performed an experiment with ECBilt for the last 1000 years using annual-resolution solar forcing (Crowley 2000). We use this experiment to compare the climatic sensitivity and signal-to-noise ratio of ECBilt to that of other models and proxy data. The forcing is based on ^{10}Be measurements from Antarctica (Bard et al. 1997), spliced into the Lean et al. (1995) record. Different scaling factors have been proposed in the literature (see Bard et al. 2000 for an overview). We use a conservative one, which results in a 0.20% decrease in total solar irradiance (TSI) for the deepest part of the Maunder Minimum (at about 1690 AD) with respect to the mean value of 1366 W/m^2. In the following we will define the solar irradiance forcing as the prescribed anomalies in TSI divided by four to account for the Earth's geometry. They have amplitudes of 0.5–1.0 W/m^2. The climatic sensitivity (or regression parameter; in °C per W/m^2) is defined as the temperature response divided by the solar forcing. The signal-to-noise ratio is given by the correlation coefficient.

Variations in global, annual-mean surface air temperature (SAT), that are associated with the solar forcing, have an amplitude of 0.1–0.2 °C in the ECBilt experiment. This implies a climatic sensitivity of 0.2, which is clearly lower than the figures given for more comprehensive GCMs of 0.4 (Cubasch et al. 1997) and 0.5 (Rind et al. 1999; henceforth RLH). Waple et al. (2002) give an empirical estimate of 0.24 for the global-mean sensitivity (for the period 1650–1850 AD), based on the temperature reconstruction of Mann et al. (1998) and the Lean et al. (1995) irradiance record. The spatial response pattern in ECBilt has highest amplitude over land in mid-high latitudes and lowest amplitude over the tropical oceans, similar to the pattern shown by Cubasch et al. (1997). A comparison of empirical and GCM-based spatial response patterns indicates reasonable similarity, although the empirical pattern has more regional detail (Waple et al. 2002).

The correlation coeffcient between global, annual-mean SAT and the solar forcing is 0.68 in the ECBilt experiment, while RHL give a value of 0.74. The signal-to-noise ratio in ECBilt is thus similar to that in GCMs, although the climatic sensitivity is too weak. The reason for this is that ECBilt also underestimates internal climatic variability (see Drijfhout et al. 1999). This aspect can be quantified in more detail by comparing latitudinal correlations obtained with ECBilt to results reported by RHL. In the tropics (16°S–16°N) the correlation for the annual-mean SAT is 0.76 (0.7 in RHL), in midlatitudes (30–60° in both hemispheres) it is 0.57 (0.5 in RHL) and in high latitudes (poleward of 60°) it is 0.2 (0.2 in RHL). The lag at which optimal correlations occur is about 4 years, with a broad peak around the optimal lag consistent with RHL.

Global, annual-mean precipitation shows a clear response to the insolation forcing in the 1000-year ECBilt experiment. The regression is about 1 cm/year per W/m^2, which is 1% of the

time-mean precipitation value. A 1% change in precipitation concurrent with 0.1–0.2 °C temperature changes seems high in comparison to IPCC figures. These indicate a 1% precipitation increase concurrent with a 1 °C temperature increase (Cubasch et al. 2001). The reason is probably that ECBilt underestimates the time-mean precipitation in the tropics. Variations in the water holding capacity of the atmosphere associated with variations in temperature seem to be the cause of the simulated correlation between precipitation and insolation.

Proxy based estimates of the correlation between temperature and solar forcing for the period 1600-present range from 0.57–0.74 for annual data (Crowley and Kim 1996) to 0.75–0.86 for decadal-mean data (Lean et al. 1995). These figures may be spurious because on the one hand, the CO_2 and solar indices correlate well, and on the other hand, the pre-anthropogenic period contains only 1–2 cycles of the dominant low-frequency component in the solar forcing (Crowley and Kim 1999). Four 1000-year reconstructions of Northern Hemisphere (NH) temperature have recently become available. They are representative for annual-mean conditions (Mann et al. 1999; Crowley and Lowery 2000) or for the warm season (Jones et al. 1998; Briffa 2000). All data can be obtained from the World Data Center for Paleoclimatology (http://www.ngdc.noaa.gov/paleo). We found the correlation of these records with the solar forcing to be 0.2–0.4 for the pre-anthropogenic interval (1000–1850 AD). This is clearly lower than the values found in ECBilt (for the same time interval). This is also true for the decadal-centennial range, as shown in Fig. 1. Both in the model and in the data there is a tendency for higher correlations for longer time scales, with overall lower values in the data than in the model.

One possible reason for this discrepancy between reconstructed and simulated records is the neglect of volcanic forcing in the model simulations. This point is illustrated in Fig. 1 by results from a second 1000-year experiment with ECBilt, using both solar and volcanic forcing (Crowley 2000). Volcanic forcing introduces additional variability uncorrelated with the solar irradiance forcing, thus reducing correlations. A possible bias in the data toward high-latitudes reduces correlations, while a bias toward the warm season increases correlations (Fig. 1). Other reasons for the model-data discrepancy might be inadequate sampling of the large-scale signal in the data or noise inherent in the biological and geological records used in the reconstructions.

We conclude that hemispheric-scale temperature and precipitation correlations in ECBilt are consistent with those found in earlier GCM studies. The temperature sensitivity is underestimated compared to earlier GCM studies, while it is on the low end of the range of sensitivities estimated by the recent IPCC Third Assessment Report (Cubasch et al. 2001). However, it is only slightly lower than an empirical estimate of the temperature response to solar forcing. Correlations seem to be overestimated in all models, in comparison to proxy data. This is partly due to the neglect of volcanic dust in the model experiments.

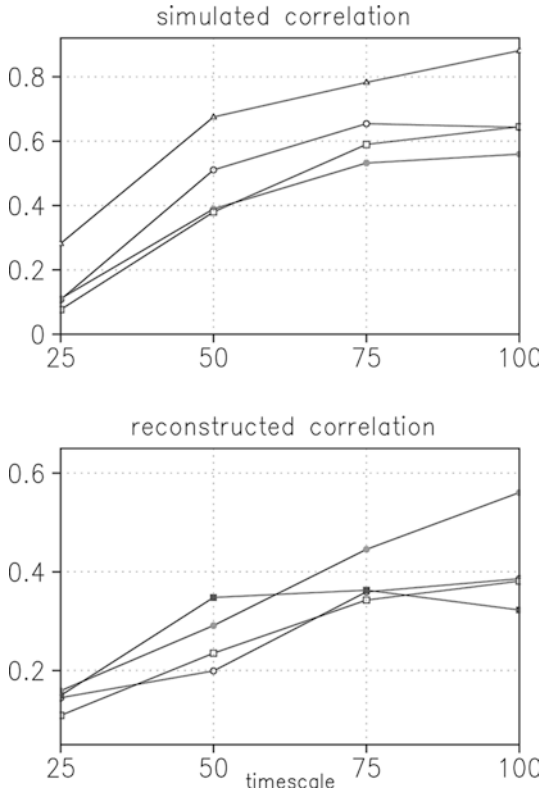

Fig. 1 The correlation with the solar irradiance forcing in two ECBilt simulations (*upper panel*): annual NH temperature in the solar-forced experiment (*triangles*) and in the solar-volcanic forced experiment (*open cicles*). Also shown are annual (*solid circles*) and summer (*open squares*) temperature for land points north of 30°N in the solar-volcanic forced experiment. The correlation for reconstructed temperatures (*lower panel*): the records of Jones et al. (1998; *open circles*), Mann et al. (1999; *solid circles*), Briffa (2000; *open squares*) and Crowley and Lowery (2000; *solid squares*). All correlations are computed over the pre-anthropogenic interval (1000–1850 AD) for different band-pass filter periods (in years)

2.3 Design of the 10,000 year experiments

Two 10,000 year simulations were made with ECBilt, one solar-orbital forced and one with orbital forcing alone. The orbital forcing for the period of 10 kyr BP (thousand years before present) up till now is due to variations in the parameters of the Earth's orbit (Berger 1978). It modifies the seasonal and geographical distribution of incoming short-wave radiation. The solar forcing is prescribed as a small modulation of the solar constant. It is assumed to be constant thoughout the year. In both experiments all other boundary conditions (orography, concentration of trace gases and tropospheric aerosols, surface characteristics) are set to their present-day values.

The solar forcing is based on the residual ^{14}C record (Stuiver et al. 1998), which is interpolated within the decades to get an annual time series. It is scaled to the Lean et al. (1995) record in such a manner that the TSI decrease for the Maunder Minimum is the same as in the forcing record used in the 1000-year experiment. This implies a scaling factor of –0.0185 W/m^2 per *permil*. The ^{14}C record and the associated solar irradiance forcing are depicted in Fig. 2. Although ^{10}Be is generally thought to be the better proxy for solar activity, at the time of running the experiments there were no high-resolution records available for the period of interest here. Instabilities of the ocean circulation have been hypothesized to cause the low-frequency variability in the residual ^{14}C record, especially in the early Holocene (Stuiver and Braziunas 1993). As any filtering of the forcing record would be arbitrary, we have chosen to apply the full record. The good agreement between the independent ^{14}C and ^{10}Be-based assessments of solar variability for the last millenium suggests that ocean variability is playing a relatively minor role in modifying the ^{14}C signal. A possible feedback of the oceanic circulation on the atmospheric ^{14}C content will be examined a-posteriori.

The combined solar-orbital record is shown in Fig. 3 (top). The long-term trend is characterized by a gradual decrease in NH summer insolation during the Holocene, especially at mid-to-high latitudes. This results in a gradual cooling of NH summers (Fig. 3, middle), a reduced land-sea contrast, reduced low-level convergence over the NH land mass and a decrease in summer monsoon precipitation (Fig. 3, bottom). The amplitude of the ECBilt response at 6 kyr BP, which is one of the foci of the Paleo Modeling Intercomparison Project (PMIP), falls in the low-middle range of the PMIP modeling results (Weber 2001; Braconnot et al. 2003).

Time-slice experiments with ECBilt show a reduction (by about 0.7 Sv) in the North Atlantic overturning circulation in response to the annual-mean orbital forcing at the mid-Holocene optimum

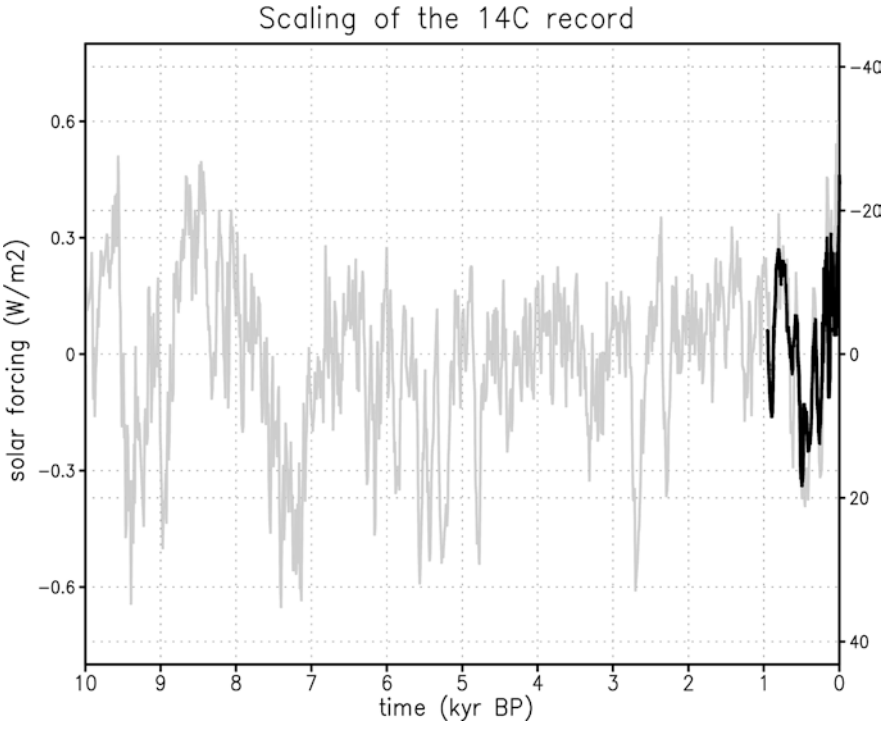

Fig. 2 Solar irradiance forcing (*grey line*) based on the residual ^{14}C record (Stuiver et al. 1998) for the last 10,000 years (*left axis*; in W/m^2). The *right axis* gives the corresponding units of *permil* of the original record. For comparison the Lean reconstruction of historic irradiance variations is extended back in time to the year 1000 AD by the independent ^{10}Be record (Bard et al. 1997) (*black line*). Time in calendar kyr BP (where 0 year BP is defined as 1950 AD)

(Braconnot et al. 2003). In the present transient experiments any orbital-forced oceanic signal is dominated by transitions which occur in the southern ocean between a 'weak overturning' and a 'strong overturning' state. The former state is characterized by a small drift in the deep ocean (of about 0.05 °C/century). Both states have a typical residence time of many millenia. All long ECBilt experiments exhibit this behavior, which was first described in a control run (Haarsma et al. 2001). As the time scale of this transitional behavior is similar to the orbital time scale, we will not consider the oceanic response to orbital forcing in the present experiments. In order to analyze the response to solar forcing, we have high-pass filtered the simulated oceanic records to remove all variability on time scales longer than 1200 years. The solar response discussed in the following sections was found to be independent of the southern-ocean overturning state.

3 The atmospheric response as a function of time scale

There is pronounced climatic variability superimposed on the orbital-forced trend, as illustrated in Fig. 3. In this and the following section we examine to what extent climatic variability is related to the irradiance forcing and how this relationship depends on the time scale. This is done by band-pass filtering the forcing and response records and then computing the lagged correlation for filter periods τ ranging from 50 to 700 years. The lag is varied over a range of 0–30 years in Sect. 3.1 (and in Sect. 4), while the range is 50 years centered around the glacier response time in Sect. 3.2. We check whether the lag at which the optimum correlation occurs is physically realistic. The statistical significance of correlations is estimated following Von Storch and Zwiers (1999) using a t test, with the number of samples given by the record length divided by the filter period. We apply a two-sided test, unless the sign of a (small) signal can be established a-priori. Focus of the following analysis is on variability on multi-decadal and longer time scales.

3.1 Temperature and precipitation

In this section we will examine the response of temperature and precipitation for different areas with spatial scales ranging from regional to hemispheric (Fig. 4). Temperature correlations are found to be small for relatively short time scales. This is due to the long response time scale of the oceans. As a result the solar irradiance forcing is integrated over time, which effectively damps the climatic response at shorter time scales. Correlations are also small regionally, e.g. for the European area (0–50°E and 35–70°N), because at small spatial scales the amount of noise in the system is relatively large. However, temperatures are very well correlated with the solar forcing at the continental or hemispheric scale. At low latitudes correlations are larger than at higher latitudes, while the same holds for summer versus winter. The regression (of 0.2–0.4 °C per W/m^2) is found not to depend sensitively on the time scale.

The NH annual-mean precipitation response can be separated into a contribution from midlatitudes (north of 30°N) and from low latitudes. At midlatitudes precipitation correlates well with temperature, which links it to the irradiance forcing. This effect is even evident for small spatial scales, although one has to go to long temporal scales to reach a correlation that is statistically significant. At low latitudes the summer (June–July–August) signal dominates the precipitation response.

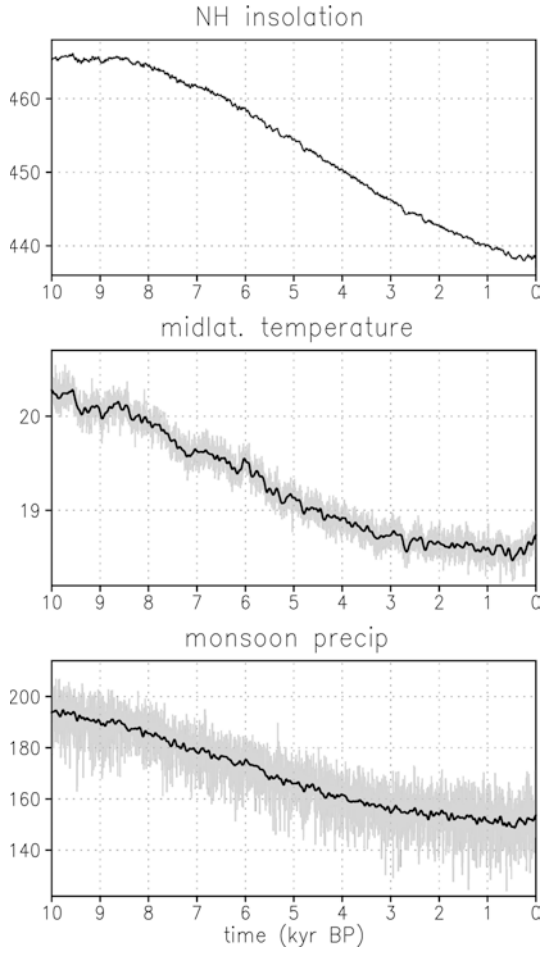

Fig. 3 NH incoming insolation (in W/m^2; *upper panel*), temperature in NH midlatitudes (in °C; *middle panel*) and monsoon precipitation over North Africa (in cm/year; *lower panel*) for June–July–August as a function of time (in kyr BP) from the solar-orbital forced ECBilt run. *Grey lines* in the *lower two graphs* give yearly values, *black lines* the 100-years low-pass filtered values

The spatial response pattern shows an increase in the African-Asian monsoon precipitation for high irradiance. The impact is only discernable at centennial and longer time scales. Over north Africa (20°W–50°E and 5–25°N) the regression is 1–2 cm/year per W/m^2. There is a slight northward shift as well, with a few tropical gridpoints (5–10°N and 10–40°E) where precipitation decreases (by about 3 cm/year per W/m^2). The negative response in the tropics seems to be a robust feature, although correlations are low here.

For the temperature as well as the precipitation records the optimum lag always lies in the range 0–20 years, with longer lags for longer time scales. We examined whether the impact of solar forcing depends on the background climatic state by separately analyzing the first and the second half of the 10,000 year simulation for all records. The results were found not to depend on the time interval.

The monsoon precipitation response seems to be due to the following mechanism. A positive radiative forcing in summer (due to a high solar irradiance) leads to stronger heating of the NH continents, an intensified large-scale flow and a stronger hydrological cycle. This mechanism is confirmed by the correlation between summer precipitation over North Africa and temperature over the NH midlatitude continents, which is 0.77 using 100-year low-pass filtered records. For the Asian monsoon this is 0.69. The mechanism described here is similar to that underlying the monsoon response to the summer orbital forcing at the mid-Holocene optimum. An indication of the sensitivity of the ECBilt model is obtained by comparing the amplitude of its response at 6 kyr BP to that of other models and proxy data. Here we assume that the strength of the relevant feedbacks is similar for centennial time scales (solar forcing) and millenial time scales (orbital forcing). In PMIP the simulated maximum difference in annual precipitation (between 6 kyr BP and present) over north Africa ranges from 5 to 40 cm/year (Joussaume et al. 1999), whereas it is 15 cm/year in ECBilt. The values found in the PMIP models seem to be on average at least a factor 2 smaller than estimates based on proxy data (Joussaume et al. 1999). The sensitivity of the African monsoon to orbital forcing is thus found to be smaller in ECBilt than in a number of other models. It is likely to be underestimated considerably compared to proxy data. Therefore we tentatively conclude that the simulated African monsoon response to solar irradiance forcing is a realistic feature, although ECBilt considerably underestimates subtropical variability.

The imprint of the solar irradiance forcing on the climatic spectra is illustrated in Fig. 5. The Fourier spectra are computed by cutting the records in overlapping segments of length 2048 years and then averaging the results. The longest period that can be resolved is 1024 years. The forcing spectrum (upper panel) is red, with spectral peaks at 80–90, 140–160 and 200–220 years (see also Stuiver and Braziunas 1993). In addition, Fig. 5 gives the spectrum of the temperature of the NH midlatitudes, which has correlations of 0.6–0.95 at time scales longer than 100 years, and of rainfall over North Africa, which has correlations of 0.3–0.6 in the same time scale range (see Fig. 4). The temperature spectrum shows increased variance for centennial time scales in the solar-orbital forced run compared to the orbital forced run. In additon, the 140–160 years and 200–220 year peaks are clearly recognizable. The precipitation spectrum is not significantly modified by the irradiance forcing.

3.2 Glacier length: a combined temperature and precipitation signal

Many proxy records represent a combined temperature and precipitation signal. As an example we analyze glacier length for three glaciers, for which a process-based model of glacier dynamics exists. Such a model can be coupled off-line to the climate model, using

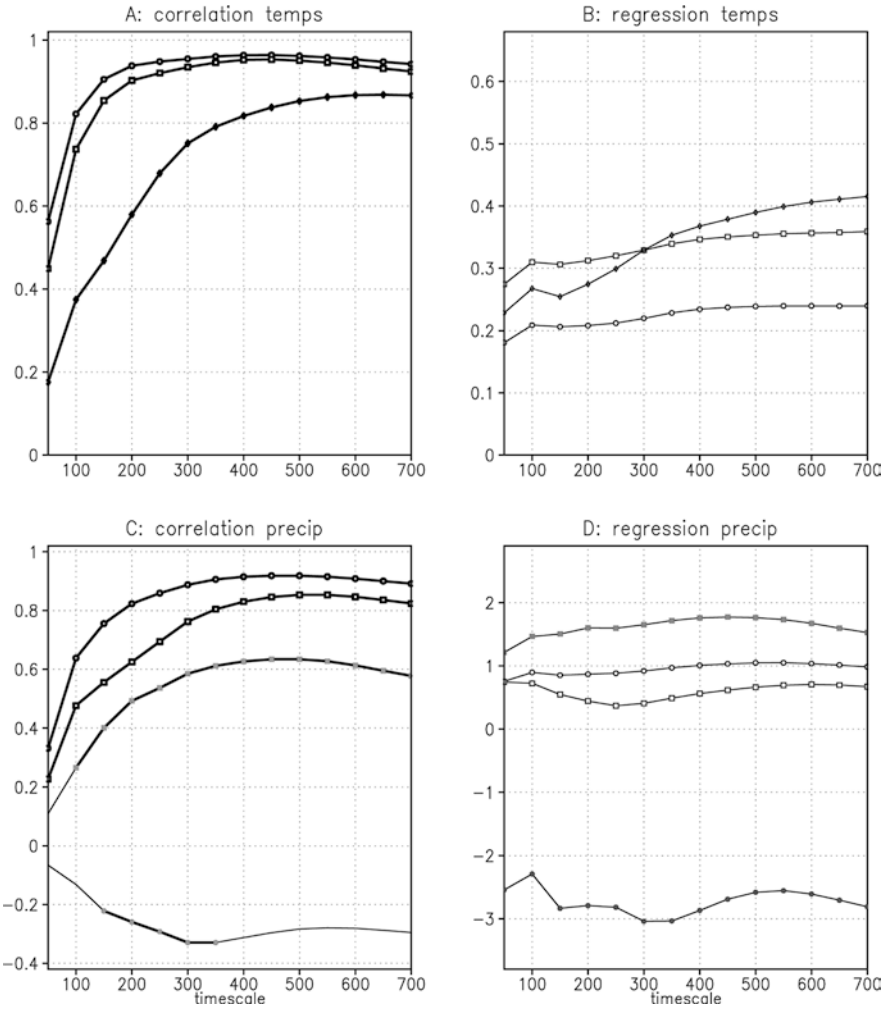

Fig. 4 **A** The correlation with the solar irradiance forcing as a function of time scale (in years) for the annual-mean temperature of the NH (*open circles*), the NH midlatitudes (*open squares*) and Europe (*diamonds*). **B** The temperature regression (in °C per W/m^2). **C** Same as **A**, but now for the precipitation of the NH (*open circles*), the NH midlatitudes (*open squares*), North Africa (*solid squares*) and equatorial North-Eastern Africa (*solid circles*). **D** The precipitation regression (in cm/year per W/m^2). Thick marked line segments in **A** and **C** denote correlations that are significant at the 10% level in a two-sided *t*-test

simulated monthly temperature and precipitation anomalies as input. The procedure has been described earlier (Reichert et al. 2002; Weber and Oerlemans 2003). ECBilt has reasonable skill in simulating the relative contributions of temperature and precipitation to the climatic forcing of the glacier model (Weber and Oerlemans 2003). However, the overall level of variability is underestimated. We consider three glaciers, ranging respectively from maritime to continental: Nigardsbreen (62°N, 7°E) in southern Norway, Rhonegletscher (47°N, 8°E) in the Swiss Alps and Abramov glacier (40°N, 72°E) in Kirghizia.

The long-term trends in glacier length in the solar-orbital forced experiment are very similar to those in the orbital forced experiment described earlier (Weber and Oerlemans 2003). Nigardsbreen, which is a very sensitive glacier, increases its length by more than 12 km during the Holocene. This is primarily due to decreasing summer temperatures. The glacier is confined to a narrow valley in the interval 10–5 kyr BP, which results in rapid expansion and pronounced variability. After 5 kyr BP a broader valley is entered. Rhonegletscher shows only a slight expansion. Abramov glacier reaches a neo-glacial maximum (of 1 km more than its present-day length) during the mid-Holocene as a result of enhanced monsoon precipitation at this time.

The correlation between glacier length and the solar forcing is shown in Fig. 6A. Glacier length variations consist of a part related to temperature and one related to precipitation. At all three locations the temperature contribution dominates the length response. The positive correlation between the solar forcing and (summer) temperature results in a negative correlation with the glacier length. For Nigardsbreen and Rhonegletscher correlations increase up to time scales of about 250 years. They decrease again for longer time scales. This is due to the precipitation contribution, as local precipitation shows a response to the solar forcing for centennial and longer time scales. Abramov glacier is situated at low latitudes, where the summer temperature correlation is higher than at Nigardsbreen and Rhonegletscher. Here the correlation increases smoothly for all time scales.

Correlations were computed separately over the first and the last 5 kyr of the simulation, in order to examine whether there are any differences between the different length ranges. The climatic forcing (on sub-millenial time scales) is similar during the two periods. The results

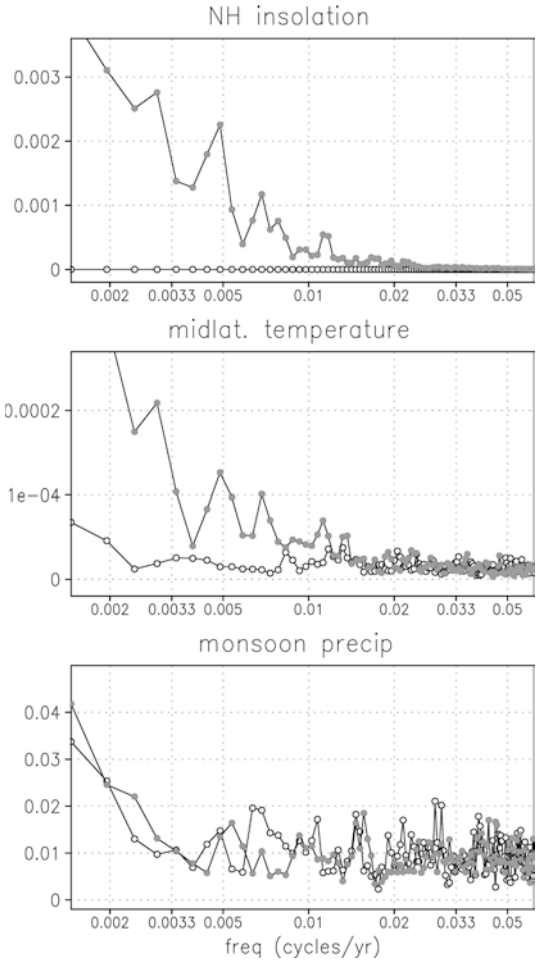

Fig. 5 Variance spectrum of the annual-mean NH incoming insolation (*upper panel*), temperature in NH midlatitudes (*middle panel*) and monsoon precipitation over North Africa (*lower panel*), refer to Fig. 3 for units. Spectra for the solar-orbital forced run are indicated with *solid circles*; spectra for the orbital forced run with *open circles*

for Nigardsbreen suggest that correlations decrease more strongly for $\tau > 250$ years in the rapid expansion phase (10–5 kyr BP), while the glacier sensitivity is much higher (Fig. 6B). For Rhonegletscher and Abramov glacier the results do not depend on the time period.

The optimal lags are shown in Fig. 6C. Their mean values (over all time scales) range from 30 year for Rhonegletscher, 60–70 years for Nigardsbreen to 75 years for Abramov glacier. The pattern of increasing time scale for Rhonegletscher, Nigardsbreen and Abramov glacier agrees with the specific response periods of each glacier (Oerlemans 2000). Nigardsbreen shows a longer lag in the early Holocene than in the later period. This is probably due to the higher sensitivity in the rapid expansion phase (Fig. 6B), which leads to larger excursions of the glacier snout. The glacier length spectra are very similar in the solar-orbital forced run and the orbital forced run. They are red, without significant periodicities. We thus find that the solar forcing excites only weak signals in glacier length. The reason for this is

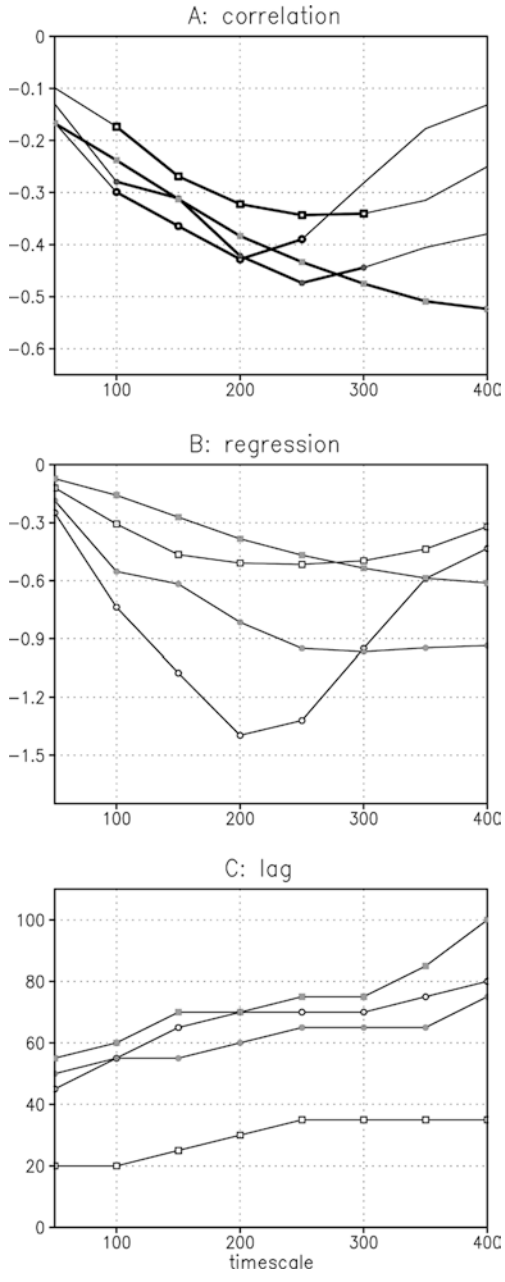

Fig. 6 **A** The correlation of glacier length with the solar irradiance forcing as a function of time scale (in year) for Nigardsbreen in the period 10–5 kyr BP (*open circles*) and in the period 5–0 kyr BP (*solid circles*), for Rhonegletscher (*open squares*) and Abramov glacier (*solid squares*). Significance indicated as in Fig. 4. **B** The regression of glacier length (in km per W/m^2). **C** The lag (in years) at which the optimal correlation occurs

that the link between the solar forcing and the local climate, which drives the glacier mass balance, is weak.

4 The ocean response as a function of time scale

4.1 The overturning circulation

We first consider the ocean response in the Atlantic basin. Figure 7 shows the simulated mean overturning

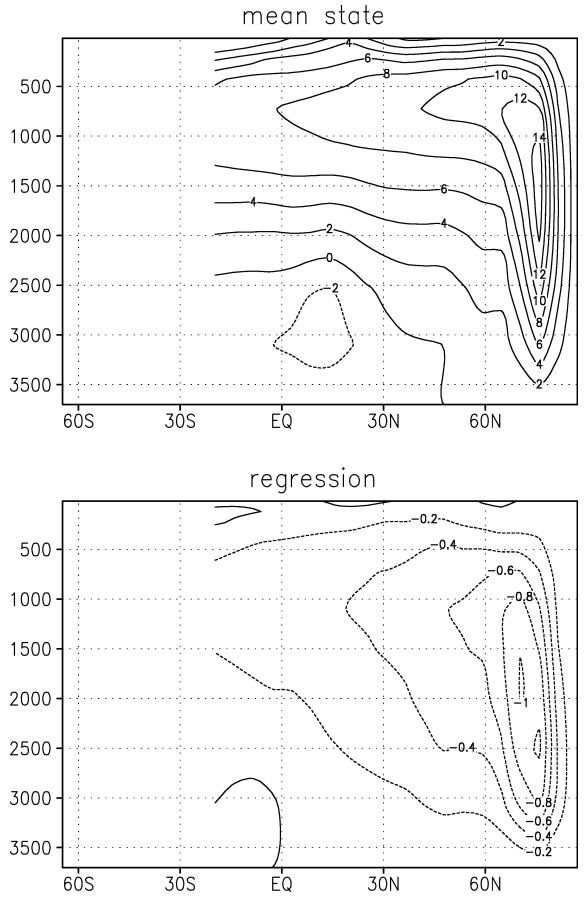

Fig. 7 The North Atlantic overturning circulation (*upper panel*; in Sv) for the present-day climate (100-year mean) as a function of depth and latitude. The regression (*lower panel*; in Sv per W/m^2) of the overturning circulation on the solar irradiance forcing for the 10,000 year experiment

stream function in the latitude-depth plane. The amount of North Atlantic Deep Water formed in the model is about 14 Sv, close to the observed value. The location of convection sites is further north than observed, which is due to a warm bias at high latitudes in ECBilt. The overturning stream function is anticorrelated with irradiance anomalies, as shown in Fig. 7. The mechanism underlying the thermohaline circulation (THC) response in ECBilt was described by Van der Schrier et al. (2002) based on a small number of 1000-year experiments, using both the Lean et al. (1995) estimate and a higher-amplitude scaling of the solar irradiance forcing. High (low) irradiance was found to lead to increased (reduced) surface temperatures in the northern North Atlantic, increased (reduced) stability of the water column and reduced (increased) deep-water formation, followed some years later by a weaker (intensified) overturning circulation.

In the present 10,000 year experiment it is possible to examine the time scale-dependence of the oceanic response to irradiance variations. Correlations and regressions for the amount of deep-water formed at high latitudes and the maximum in the overturning stream function are shown in Fig. 8. They have their most negative values for time scales between 150–300 years. For time scales longer than 300 years correlations are not statistically significant, given the number of samples in the present experiment. Optimal correlations occur at a lag of 0 years (deep-water formation) and about 10 years (THC maximum). The spatial response patterns (not shown) are similar for different band-pass filter periods, with highest amplitudes between 150–300 years.

These results indicate that the assumption of a direct response to the solar irradiance forcing only holds for time scales longer than a few hundred years. The asymptotic value (of about –0.8 Sv per W/m^2) for the THC response is consistent with the equilibrium response found in ECBilt time-slice experiments for the mid-Holocene optimum (Braconnot et al. 2003), when the annual-mean orbital forcing had similar amplitude as the solar irradiance forcing. For τ between 150–300 years, internal feedback processes seem to play an important role.

We now consider the oceanic surface forcing, focusing on those terms in the heat and freshwater fluxes that can be considered as external forcing terms. In the coupled system the heat flux consists of the absorbed shortwave radiation and the air-sea heat exchange (net longwave radiation, latent and sensible heat). The freshwater flux consist of precipitation, runoff, evaporation and a small contribution from brine rejection. Terms that are not modified by the ocean circulation can be considered as 'external' forcing terms of the ocean component. These are the shortwave radiation term SW in the heat flux and the contribution of precipitation and runoff $P + R$ to the freshwater flux. Correlations for the northern North Atlantic (north of 45°N) are shown in Fig. 8C.

At sub-centennial time scales the *absorbed* shortwave radiation is not well correlated with the *incoming* shortwave radiation, because changes in sea-ice coverage result in albedo variations that are not correlated with the incoming radiation. However, at longer time scales sea-ice closely follows the insolation. This results in correlations that increase smoothly with τ. Precipitation and run-off also show increasing correlation for increasing timescale, consistent with the curves shown in Sect. 3. In order to quantitatively compare the two terms we have computed the regression (Fig. 8D) in terms of the buoyancy forcing due to the absorbed shortwave radiation and precipitation plus run-off, respectively. Here a linear approximation of the equation of state was used. The buoyancy forcing is dominated by the heat flux term, with a smaller contribution from the freshwater flux term. It is clear that both SW and $P+ R$ result in negative (positive) buoyancy forcing anomalies for high (low) irradiance, which correlate increasingly well for longer time scales. The surface forcing thus cannot explain the time scale-dependence of the THC response.

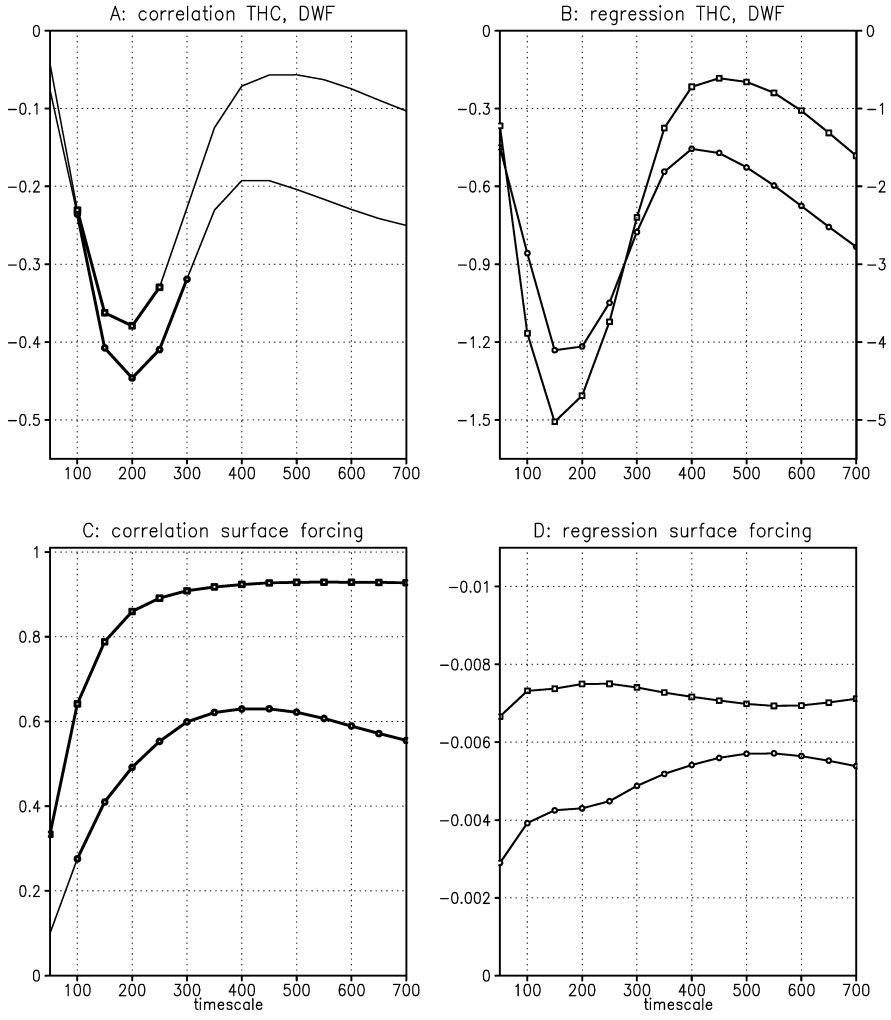

Fig. 8 **A** The correlation of the THC maximum (*circles*) and the rate of deep-water formation in the northern Atlantic (north of 45°N; *squares*) with the solar irradiance forcing as a function of time scale (in years). Significance indicated as in Fig. 4. **B** The regression of the THC maximum (*left axis*; in Sv per W/m^2) and the rate of deep-water formation (*right axis*; in percentage of the mean rate per W/m^2). **C** Same as in **A**, but now for the surface forcing of the northern Atlantic: absorbed shortwave radiation (*squares*), precipitation plus run-off (*circles*). **D** The regression of the associated *buoyancy forcing* (in kg/m^3 per year per W/m^2)

4.2 Temperature, salinity and advective feedbacks

It seems likely that advective feedback processes are important for the occurrence of a preferred time scale of about 200 years. A reduction (intensification) of the THC results in anomalous advection of temperature and salinity. This modulates the density field and thus the density contrast between high and low latitudes, which again has a direct effect on the strength of the THC (Hughes and Weaver 1994; Rahmstorf 1996; Thorpe et al. 2001). We will first consider the ocean temperature and salinity response to the irradiance forcing, examining the northern North Atlantic, the midlatitude North Atlantic (20–45°N) and the tropical Atlantic (20°S–20°N). Figure 9 gives correlations and regressions for the upper ocean (depths 0–80 m) and the deeper levels (depths below 80 m). Changes in the temperature and salinity can be due to changes in the surface forcing as well as changes in the ocean transports. Figure 8 gives an indication of the time-scale dependence of these processes, assuming that the THC strength is a reasonable measure of the zonal-mean meridional transport (more detailed output of advection and diffusion terms was not available).

The surface heat and freshwater fluxes result in warmer and fresher surface fields everywhere in the Atlantic Ocean, given high irradiance anomalies. A reduced THC transports less surface water northward, while the salty and warm water that is transported northward is exposed longer to net precipitation and cooling. This contributes to the freshening of the surface water of the northern ocean, but counteracts the warming. The upper-ocean temperature response is dominated everywhere by the surface forcing. The shape of the upper-ocean salinity correlation curve for the northern North Atlantic illustrates that the advection term dominates over the surface flux term. Correlations are optimal, albeit weak, between 150–300 years. At midlatitudes (and in the tropics, not shown) the upper-ocean salinity curve is similar, but has the reversed sign as expected. The deep-ocean response is primarily determined by advection effects, both for temperature and salinity. Given a high irradiance and reduced THC, the deep ocean freshens at high latitudes while it warms and becomes more saline at lower latitudes.

It is possible to follow the propagation of salinity and temperature anomalies around the THC loop by considering the correlation between irradiance and the

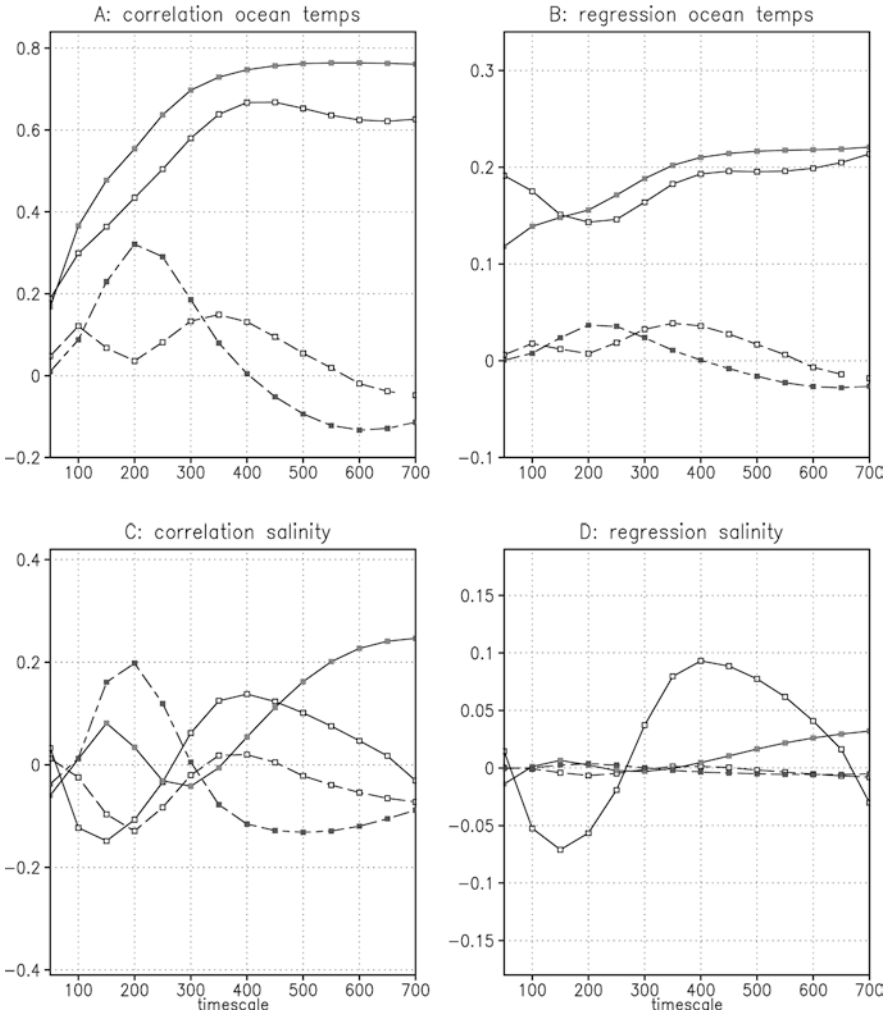

Fig. 9 **A** The correlation of surface and deep temperature with the solar irradiance forcing as a function of time scale (in years): northern Atlantic (north of 45°N; *open squares*) and mid Atlantic (20–45°N; *solid squares*). The surface levels (depths 0–80 m) are indicated by *solid lines*, while the lower levels (depths below 80 m) are indicated by *dashed lines*. **B** The temperature regression (in °C per W/m^2). **C** Same as **A**, but now for salinity. **D** The salinity regression (in PSU per W/m^2). Correlations are only significant (at the 10% level in a two-sided test) in the case of surface temperatures (all time scales) and the mid Atlantic deep-ocean temperature (in the range 150–250 years)

zonal-mean fields for the 150–300 years band-pass filtered records for different lags. Figure 10 shows the results for the salinity field. High insolation and a reduced THC initially results in a fresh anomaly at all depths north of 45°N and relatively saline water south of 45°N (Fig. 10, lag 20 years). The overturning circulation transports these anomalies southward in the deep ocean (lag 60 years), while a positive anomaly starts to develop at the most northern latitudes (lag 100 years). At lag 140 years the negative anomaly is still recognizable in the subtropical deep ocean. It does not propagate across the equator, but decays within 200 years (lags 180 and 220 years). The correlation between the zonal-mean temperature field and the insolation (not shown) gives similar results for lags of 20 and 60 years. However, the deep-ocean temperature signal is weaker than the salinity signal. The temperature signal is also less persistent and disappears for increasing lags. (A correlation between the overturning maximum and the zonal-mean salinity and temperature fields gives similar patterns, but with stronger correlations and reversed sign.)

The anomalous salinity and temperature fields obviously modify the meridional density contrast $\Delta\rho$. Figure 11 shows the correlation between $\Delta\rho$ and the solar irradiance forcing as a function of the time scale. Here the contrast between the depth-mean density of the northern and midlatitude Atlantic boxes has been used. Similar results are found for the contrast between the northern and tropical Atlantic boxes. Figure 11 also shows results for the density contrast associated with salinity differences $\Delta\rho_S$ and that associated with temperature differences $\Delta\rho_T$. Salinity anomalies, with $\Delta\rho_S$ primarily determined by the deep ocean, are found to dominate. Both the northern and the midlatitude (tropical) boxes contribute to $\Delta\rho_S$ (compare Fig. 9C). It is not surprising that correlations are again largest in the time scale range 150–300 years, as advective process dominate any change in deep-ocean salinity. Anomalies in $\Delta\rho$ in turn reinforce the THC response. This is illustrated by a direct correlation between the density contrast and the THC maximum, which shows that a linear relation indeed holds very well on centennial and longer time scales.

4.3 A loop-oscillator mode

When summarizing the analysis we conclude that the solar irradiance forcing gives rise to an initial THC

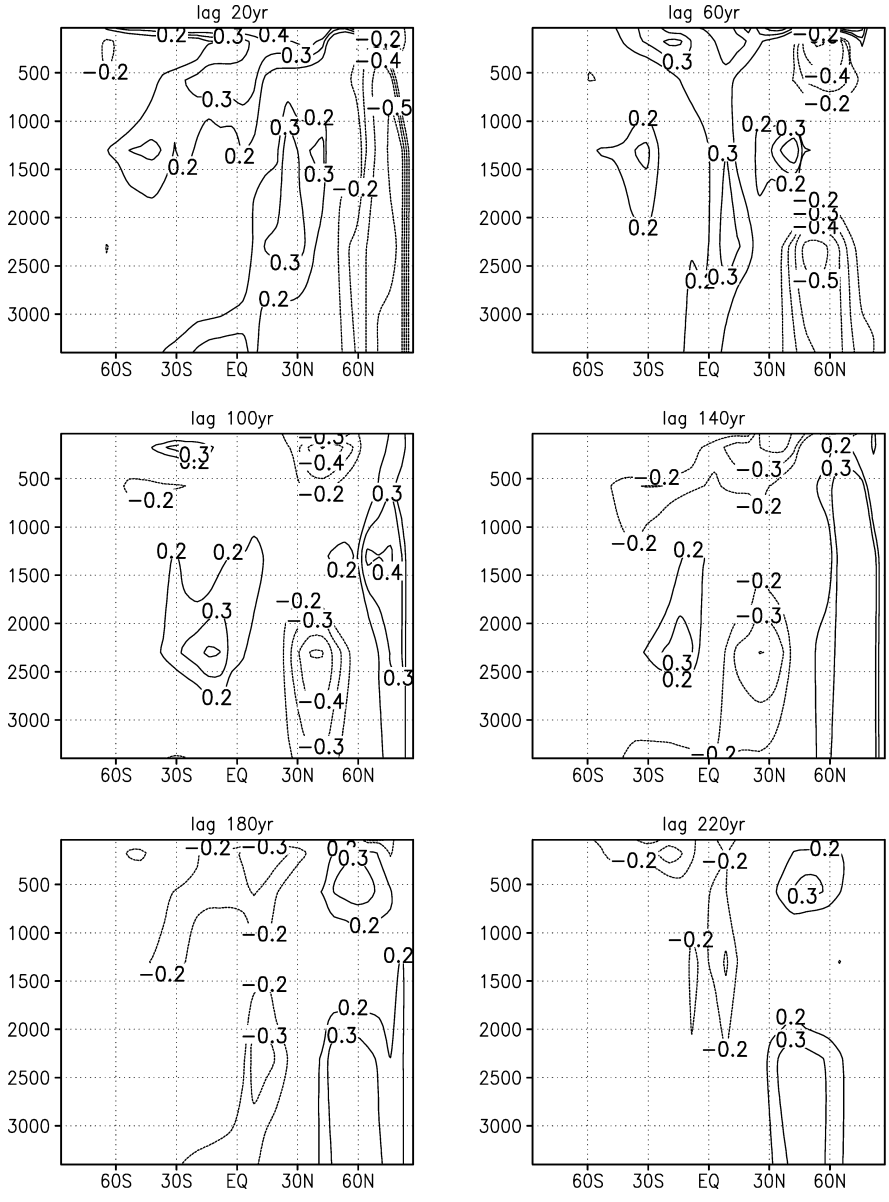

Fig. 10 Lagged correlations of the zonal-mean salinity field in the Atlantic Ocean with the solar irradiance forcing for the 150–300 year band-pass filtered records. Negative contours are *dashed*

response, which is driven by surface temperature anomalies. The THC response in turn generates salinity (and density) anomalies. This well-known salinity-advection feedback is a positive feedback on the THC response at any forcing time scale. High-latitude salinity anomalies propagate southward in the deep ocean, thus modulating the north-south density contrast with a delay of 70–150 years. If the irradiance forcing has changed sign by this time (i.e. has a periodicity in the range 150–300 years), then this is again a positive feedback on the THC response. We will term this the delayed salinity-advection feedback. In the ECBilt experiment salinity anomalies propagate around part of the THC loop, before they disappear due to diffusion and zonal spreading. Propagation and decay time scales thus set the preferred time scale range of 150–300 years, which clearly is to a certain extent model-dependent. We believe that the present analysis gives sufficient support to the delayed salinity-advection feedback as the mechanism underlying the occurrence of an optimal time scale of covariance between the THC and irradiance variations, although it is not a rigorous proof.

Earlier model studies have shown that loop-oscillator modes can be excited by white-noise freshwater forcing. A 320-year mode was found by Mikolajewicz and Maier-Reimer (1990) by applying spatially coherent noise in a 3-D ocean model forced by mixed boundary conditions. This resulted in salinity anomalies propagating around the full Atlantic loop. Mysak et al. (1993) found a 200-year mode in a 2-D ocean model coupled to a moist EBM. Here salinity anomalies were only advected around a partial THC loop. These centennial modes are essentially 2-D in the latitude-depth plane (Sirkes and Tziperman 2001), which sets them apart from the multi-decadal 3-D modes involving the gyre circulation. By using continuation techniques Te Raa

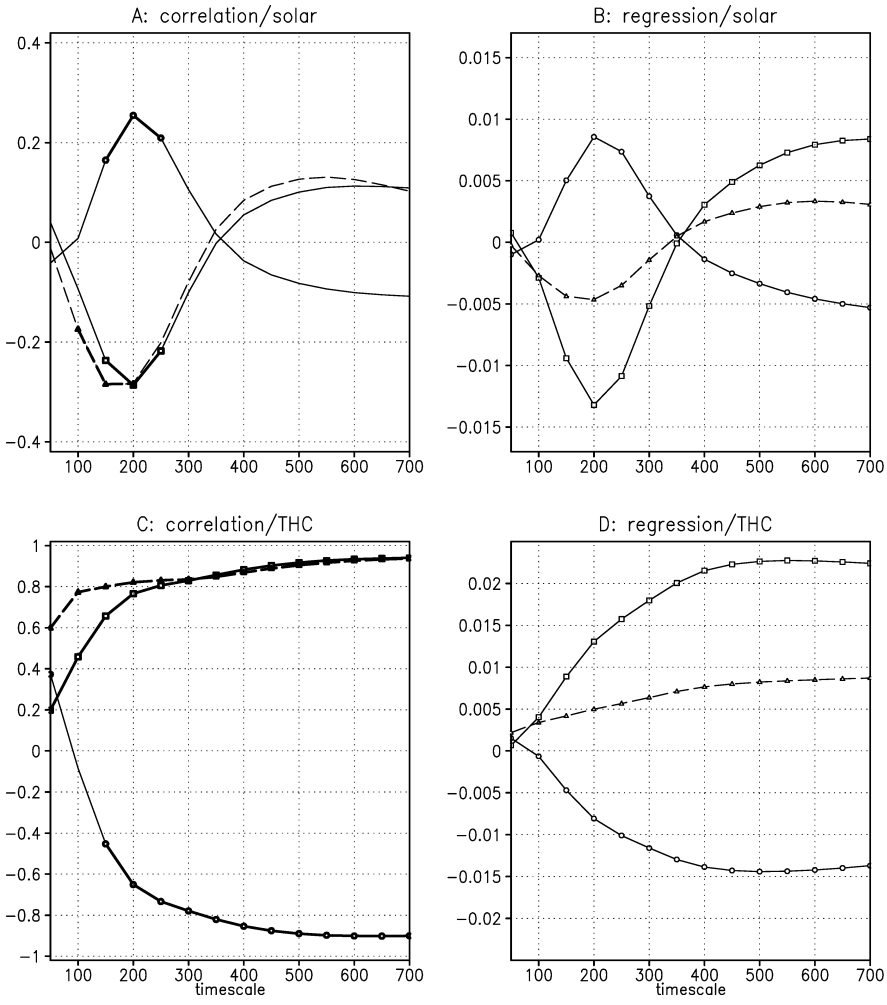

Fig. 11 **A** The correlation of the Atlantic north-south density contrast with the solar irradiance forcing as a function of time scale (in years): variations in the density contrast due to temperature variations (*circles*), due to salinity variations (*squares*) and due to both temperature and salinity variations (*dashed – triangles*). Significance indicated as in Fig. 4, but now from a one-sided *t*-test. **B** The regression of the density contrast (in kg/m^3 per W/m^2). **C** Same as in **A**, but now for the correlation with the THC maximum. **D** The regression (in kg/m^3 per Sv)

and Dijkstra (2003) performed a linear stability analysis of the ocean circulation in a single-hemispheric basin. They identified a multi-decadal 3-D mode as well as a centennial 2-D mode, with its time scale set by the mean-state overturning time scale. In contrast to earlier authors (Mikolajewicz and Maier-Reimer 1990; Mysak et al. 1993), Te Raa and Dijkstra (2003) found that the centennial loop-oscillator mode is too strongly damped to be identified in time-integrations with white-noise forcing.

Based on these earlier results we hypothesize that the solar forcing excites a strongly damped mode of variability in the THC. This mode is evident in the THC spectrum (Fig. 12), which shows a significant peak at time scales of 200–250 years. Such a peak is absent in the reference run without solar irradiance forcing. Although the preferred range of time scales coincides with an identified peak in the solar forcing spectrum of 200–220 years (Stuiver and Braziunas 1993), it is not clear a priori that the periodicity of the forcing is essential to excite this mode. An alternative is that the enhanced noise levels in the solar-forced run are sufficient to excite this mode, as some earlier studies seem to indicate. As the presently used solar forcing acts directly on the sea surface temperatures, it is probably fairly efficient.

In the Southern and Indian oceans the correlation between the THC and solar irradiance shows a similar time-scale dependence as in the Atlantic Ocean. In the Southern Ocean the negative overturning cell has maximum correlation of 0.40 at $\tau \simeq 300$ years (at a lag of about 20 years). This gives rise to a peak in the THC spectrum, which is absent in the control run. In the Indian Ocean the maximum correlation is 0.34 (at zero lag) for $\tau \simeq 250$ years, which is too low to generate a spectral peak. The preferred range of time scales found for the different basins is consistent with estimates of the overturning time scale, based on the overturning maximum divided by the volume of the water mass. This is about 300 years for the Atlantic Ocean and about 400 years for the Southern and Indian oceans. In the Pacific Ocean there is no signficant THC response to irradiance variations.

5 Discussion and conclusions

An insolation forcing of 0.5–1 W/m^2, due to solar irradiance variations, gives rise to significant climatic signals in a 10,000 year simulation with the ECBilt

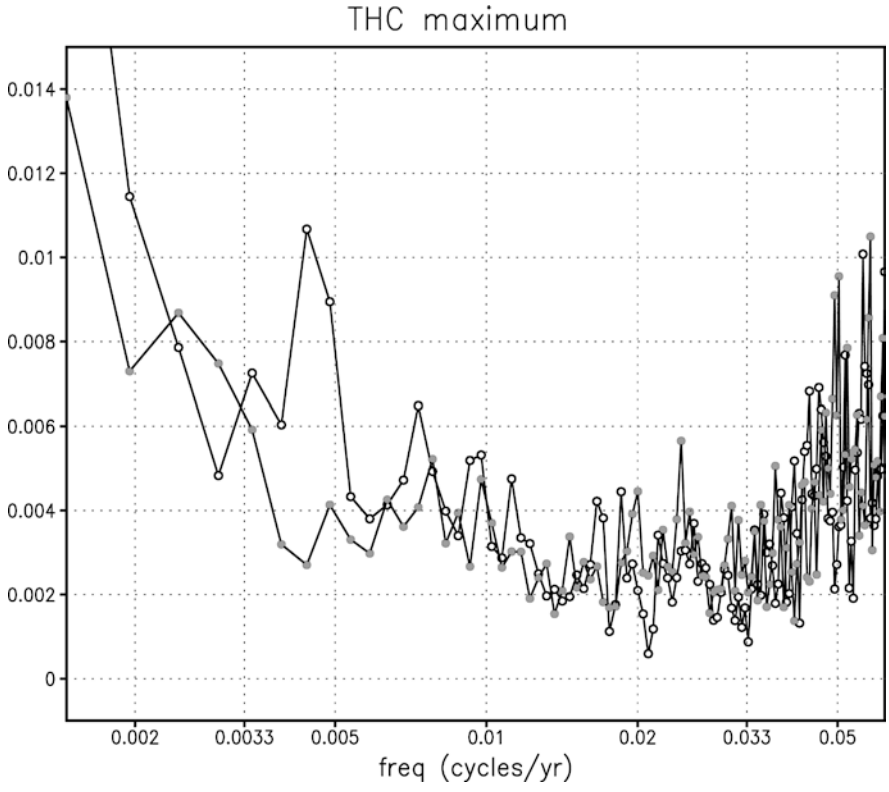

Fig. 12 Variance spectrum of the maximum of the North Atlantic overturning circulation (in Sv^2) in the solar-orbital forced run (*open circles*) and orbital forced run (*solid circles*). The solar forcing excites an internal mode of the ocean circulation with a time scale of 200–250 years

model. Temperature variations reflect the primary response of the climate system. They in turn result in midlatitude precipitation variations through changes in the atmospheric water holding capacity. In addition, variations in summer heating over the NH midlatitude continents result in changes in the large-scale atmospheric flow and associated changes in the African-Asian monsoon precipitation. The effect is similar to the climatic response to the orbital forcing of enhanced summer heating in the early Holocene, but much smaller in amplitude. Temperature and precipitation variations correlate increasingly well with the applied forcing for longer time scales and larger spatial scales. Climatic spectra show a clear imprint of the solar forcing spectrum, when correlations are higher than about 0.7.

The assumption of a direct response, attenuated at shorter time scales by the thermal inertia of the oceans, is thus found to be valid for atmospheric variables. Proxy temperature records for the last millenium seem to confirm this model result. We note that correlations in ECBilt (as well as earlier GCM studies) seem to be overestimated compared to these data. This is partly due to the neglect of volcanic dust forcing, which introduces additional variability into the climate system uncorrelated with the solar irradiance forcing. Proxy precipitation records resolving centennial-scale variability indicate a positive correlation between irradiance and the summer monsoon over North Africa (Neff et al. 2001) as well as India (Gupta et al. 2003). At the same time, equatorial east Africa was relatively dry during periods of high irradiance (Verschuren et al. 2000). Uncertainties inherent in radiocarbon dating inhibit a detailed time scale analysis of these records. These data studies support the intensified monsoon precipitation in the African-Asian subtropics and arid periods in equatorial Africa concurrent with high irradiance as found in the ECBilt simulation. The model results indicate that the monsoon response can only be identified at centennial and longer time scales.

Many proxy records reflect a combined temperature and precipitation signal. As an example glacier length was considered for three specific sites. This showed that the opposing effects of temperature and precipitation on glacier length can result in correlations that are only significant in a limited time scale range. Lags range from 20–100 years, depending on the time scale and the glacier characteristics. The correlation with the irradiance forcing was found to be too small to have an impact on the length spectra.

Irradiance variations over the oceans result in sea surface temperature variations, consistent with observational studies (White et al. 1998). In the North Atlantic Ocean this leads to changes in the amount of deep water formed at high latitudes and the strength of the overturning circulation. The correlation between the THC and the solar forcing peaks between 150–300 years. A further analysis shows that the mechanism underlying the occurrence of a preferred range of time scales is based on the advection of salinity anomalies around part of the THC loop, which modifies the north-south density contrast. This constitutes a positive feedback on the THC response, when the period of the

forcing is consistent with the propagation time scale of the salinity anomalies. Although the correlation is relatively small (–0.43), this feedback mechanism gives rise to a strong peak in the THC spectrum at time scales of 200–250 years. Such a spectral peak is absent in the reference simulation, indicating that the solar forcing excites a strongly damped internal mode of the THC.

At high latitudes the primary sea surface temperature response to the solar forcing is diminished by the THC response in the time scale band 150–300 years. At the same time the THC response leads to a substantial signal in the sea surface salinity field. Sea-ice follows low-frequency irradiance variations, but does not play an active role in the oceanic feedback processes. A significant THC response to the irradiance forcing was found earlier by Cubasch et al. (1997). In their model experiment the correlation is much larger (–0.8 over all time scales), which results in a temperature correlation at high latitudes that is even negative.

The correlation found in the ECBilt simulation implies that irradiance variations explain 10–20% of THC variations. The present results therefore do not support the view of a THC increase concurrent with every cold climatic period associated with low irradiance, and vice versa for high irradiance. This is, to a certain extent, consistent with the ambiguous evidence for THC changes during the Holocene in marine records (Broecker 2000; Keigwin and Boyle 2000; Van de Plassche et al. 2003). The present results do support the notion of a centennial mode in the THC, which is excited by irradiance variations. This mode is essentially 2-D in the latitude-depth plane. This sets it apart from the multi-decadal modes involving the horizontal gyres, which have been associated with solar irradiance forcing as well (Waple et al. 2002). Centennial loop-oscillator modes have been identified earlier in ocean models by applying random-noise freshwater forcing (Mikolajewicz and Maier-Reimer 1990; Mysak et al. 1993). They have not been described before in connection with solar forcing. Bond et al. (2001) report variations in ice-rafted debris in North Atlantic sediment records for the Holocene, which show maximum correlations with solar irradiance variations in a centennial and a millenial time scale band. There is no evidence in ECBilt for a significant response at millenial time scales. The present model results do provide a possible explanation for a centennial signal in oceanic fields, namely through a resonant THC response that amplifies the weak solar forcing.

Finally, we note that it has been hypothesized that the low-frequency peaks in the ^{14}C spectrum are due to variations in the ventilation rate of the ocean (Stuiver and Braziunas 1993). The present model results indicate that the 200 year peak cannot be regarded as an 'ocean-mode', as such a mode is absent in the reference integration. It must be, at least partly, due to solar irradiance variability. However, the ocean response could amplify or diminish the 'solar-mode' peak in the ^{14}C spectrum. Experiments with atmosphere–ocean models, which include a full carbon cycle, are needed to determine the sign of this possible feedback on the atmospheric ^{14}C content.

Acknowledgements We would like to thank Hans Oerlemans for running his glacier models and Sybren Drijfhout, Lianke te Raa and Rob van Dorland for stimulating discussions and comments on earlier drafts of this study.

References

Bard E, Raisbeck GM, Yiou F, Jouzel J (1997) Solar modulation of cosmogenic nuclide production over the last millennium: comparison between ^{14}C and ^{10}Be records. Earth Plan Sci Lett 150: 453–462

Bard E, Raisbeck G, Yiou F, Jouzel J (2000) Solar irradiance during the last 1200 years based on cosmogenic nuclides. Tellus 52B: 985–992

Berger A (1978) Long-term variations of daily insolation and Quaternary climatic changes. J Atmos Sci 35: 2362–2367

Bond G, Kromer B, Beer J, Muscheler R, Evans MN, Showers W, Hoffmann S, Lotti-Bond R, Hajdas I, Bonani G (2001) Persistent solar influence on North Atlantic climate during the Holocene. Science 294: 2130–2136

Braconnot P, Harrison SP, Joussaume S, Hewitt CD, Kitoh A, Liu B, Otto-Bliesner B, Syktus J, Weber SL (2003) Evaluation of PMIP coupled ocean-atmosphere simulations of the mid-Holocene. In: Battarbee RW, Gasse F, Stickley CE (eds) Past climate variability through Europe and Africa. Kluwer Academic Publishers, Dordrecht, The Netherlands

Briffa KR (2000) Annual variability in the Holocene: interpreting the message of ancient trees. Quat Sci Rev 19: 87–105

Broecker WS (2000) Was a change in the thermohaline circulation responsible for the Little Ice Age? Proc Natl Acad Sci USA 97: 1339–1342

Claussen M, Mysak LA, Weaver AJ, Crucifix M, Fichefet T, Loutre M-F, Weber SL, Alcamo J, Alexeev VA, Berger A, Calov R, Ganopolski A, Goosse H, Lohman G, Lunkeit F, Mokhov II, Petoukhov V, Stone P, Wang Z (2002) Earth system models of intermediate complexity: closing the gap in the spectrum of climate system models. Clim Dyn 18: 579–586

Crowley TJ (2000) Causes of climate change over the past 1000 years. Science 289: 270–277

Crowley TJ, Kim K-Y (1996) Comparison of proxy records of climate change and solar forcing. Geophys Res Lett 23: 359–362

Crowley TJ, Kim K-Y (1999) Modeling the temperature response to forced climate change over the last six centuries. Geophys Res Lett 26: 1901–1904

Crowley TJ, Lowery TS (2000) How warm was the Medieval Warm Period? Ambio 29: 51–54

Cubasch U, Voss R, Hegerl GC, Waskewitz J, Crowley TJ (1997) Simulation of the influence of solar radiation variations on the global climate with an ocean-atmosphere general circulation model. Clim Dyn 13: 757–767

Cubasch U, Meehl GA, Boer GJ, Stouffer RJ, Dix M, Noda A, Senior CA, Raper S, Yap KS (2001) Projections of future climate change. In: Houghton JT et al. (eds) Climate change 2001: The Scientific Basis. Cambridge University Press, Cambridge, UK, p 881

Drijfhout SS, Haarsma RJ, Opsteegh JD, Selten FM (1999) Solar-induced versus natural variability in a coupled climate model. Geophys Res Lett 26: 205–208

Gupta AK, Anderson DM, Overpeck JT (2003) Abrupt changes in the Asian southwest monsoon during the Holocene and their links to the North Atlantic Ocean. Nature 421: 354–357

Haarsma RJ, Opsteegh JD, Selten FM, Wang X (2000) Rapid transitions and ultra-low frequency behaviour in a 40 kyr integration with a coupled AOGCM. Clim Dyn 17: 559–570

Hughes T, Weaver A (1994) Multiple equilibria of an asymmetric two-basin model. J Phys Oceanogr 24: 1383–1397

Jones PD, Briffa KR, Barnett TP, Tett SFB (1998) High-resolution paleoclimatic records for the last millenium: interpretation, integration and comparison to control-run temperatures. The Holocene 8: 455–471

Joussaume S, 33 co-authors (1999) Monsoon changes for 6000 years ago: results of 18 simulations from PMIP. Geophys Res Lett 26: 859–862

Keigwin LD, Boyle EA (2000) Detecting Holocene changes in thermohaline circulation. Proc Natl Acad Sci USA 97: 1343–1346

Lean J, Beer J, Bradley R (1995) Reconstruction of solar irradiance since 1610: implications for climate change. Geophys Res Lett 19: 3195–3198

Mann ME, Bradley RS, Hughes MK (1998) Global-scale temperature patterns and climate forcing over the past six centuries. Nature 392: 779–787

Mann ME, Bradley RS, Hughes MK (1999) Northern Hemisphere temperatures during the past millenium: inferences, uncertainties and limitations. Geophys Res Lett 26: 759–762

Mikolajewicz U, Maier-Reimer E (1990) Internal secular variability in an ocean general circulation model. Clim Dyn 4: 145–156

Mysak LA, Stocker TF, Huang F (1993) Century-scale variability in a randomly forced, two-dimensional thermohaline circulation model. Clim Dyn 8: 103–116

Neff U, Burns SJ, Mangini A, Mudelsee M, Fleitmann D, Matter A (2001) Strong coherence between solar variability and the monsoon in Oman between 9 and 6 kyr ago. Nature 411: 290–293

Oerlemans J (2000) Holocene glacier fluctuations: is the current rate of retreat exceptional? Ann Glaciol 31: 39–44

Opsteegh JD, Haarsma RJ, Selten FM, Kattenberg A (1998) ECBILT: a dynamic alternative to mixed boundary conditions in ocean models. Tellus 50A: 348–367

Rahmstorf S (1996) On the freshwater forcing and transport of the Atlantic thermohaline circulation. Clim Dyn 12: 799–811

Reichert BK, Bengtsson L, Oerlemans J (2002) Recent glacier retreat exceeds internal variability. J Clim 15: 3069–3081

Renssen H, Goosse H, Fichefet T, Campin J-M (2001) The 8.2 kyr BP event simulated by a global atmosphere-sea-ice-ocean model. Geophys Res Lett 28: 1567–1570

Renssen H, Brovkin V, Fichefet T, Goosse H (2003) Holocene climatic instability during the termination of the African Humid Period. Geophys Res Lett (in press)

Rind D, Lean J, Healy R (1999) Simulated time-dependent climate response to solar radiative forcing since 1600. J Geophys Res 104: 1973–1990

Shindell DT, Schmidt GA, Mann MA, Rind D, Waple A (2001) Solar forcing of regional climate change during the Maunder Minimum. Science 294: 2149–2152

Sirkes Z, Tziperman E (2001) Identifying a damped oscillatory thermohaline mode in a general circulation model using an adjoint model. J Phys Oceangr 31: 2297–2806

Stuiver M, Braziunas TF (1993) Sun, ocean, climate and atmospheric $^{14}CO_2$: an evaluation of causal and spectral relationships. The Holocene 3: 289–305

Stuiver M, Reimer PJ, Bard E, Beck JW, Burr GS, Hughen KA, Kromer B, McCormac G, van der Plicht J, Spurk M (1998) Intcal98 radiocarbon age calibration, 24,000-0 cal BP. Radiocarbon 40: 1041–1083

Te Raa LA, Dijkstra HA (2003) Modes of internal thermohaline variability in a single-hemispheric ocean basin. J Mar Res 61: 491–516

Thorpe RB, Gregory JM, Johns TC, Wood RA, Mitchell JFB (2001) Mechanisms determining the Atlantic thermohaline circulation response to greenhouse gas forcing in a non-flux-adjusted coupled climate model. J Clim 14: 3102–3116

Tourpali K, Schuurmans CJE, van Dorland R, Steil B, Bruhl C (2003) Stratospheric and tropospheric response to enhanced UV radiation: a model study. Geophys Res Lett 30: 1231–1234

Tuenter E, Weber SL, Hilgen FJ, Lourens LJ (2003) The response of the African summer monsoon to remote and local forcing due to precession and obliquity. Global Planet Change 36: 219–235

Van de Plassche O, van der Schrier G, Weber SL, Gehrels WR, Wright AJ (2003) Sea-level variability in the northwest Atlantic during the past 1500 years: a delayed response to solar forcing? Geophys Res Lett 30: 17,558–17,561

Van der Schrier G, Weber SL, Drijfhout SS (2002) Sea level changes in the North Atlantic by solar forcing and internal variability. Clim Dyn 19: 435–447

Verschuren D, Laird KR, Cumming BF (2000) Rainfall and drought in equatorial east Africa during the past 1,100 years. Nature 403: 410–414

Von Storch H, Zwiers F (1999) Statistical analysis in climate research. Cambridge University Press, Cambridge, UK, pp 484

Waple AM, Mann ME, Bradley RS (2002) Long-term patterns of solar irradiance forcing in model experiments and proxy based surface temperature reconstructions. Clim Dyn 18: 563–578

Weber SL (2001) The impact of orbital forcing on the climate of an intermediate-complexity coupled model. Global Planet Change 30: 7–12

Weber SL, Oerlemans J (2003) Holocene glacier variability: three case studies using an intermediate-complexity climate model. The Holocene 13: 353–363

White WB, Cayan DR, Lean J (1998) Global upper ocean heat storage response to radiative forcing from changing solar irradiance and increasing greenhouse gas/aerosol concentrations. J Geophys Res 103: 21,355–21,366